

---

# ADAPTIVE REGULARIZATION FOR LARGE-SCALE SPARSE FEATURE EMBEDDING MODELS

Mang Li\*, Wei Lyu\*

Institute of Intelligent Technology  
Alibaba International Digital Commerce Group  
Hang Zhou, China  
{mang.ll, lw386934}@alibaba-inc.com

## ABSTRACT

The one-epoch overfitting problem has drawn widespread attention, especially in CTR and CVR estimation models in search, advertising, and recommendation domains. These models which rely heavily on large-scale sparse categorical features, often suffer a significant decline in performance when trained for multiple epochs. Although recent studies have proposed heuristic solutions, they have not clearly identified the fundamental cause of this phenomenon. In this work, we provide a theoretical analysis that explains why overfitting occurs in models that use large-scale sparse categorical features. Based on this analysis, we propose an adaptive regularization method to address it. Our approach not only prevents the severe performance degradation observed during multi-epoch training, but also improves model performance within a single epoch. This method has already been deployed in online production systems.

## 1 INTRODUCTION

Click-through rate (CTR) and conversion rate (CVR) estimation are critical for advertising, search and recommendation (ASR) applications. E-commerce platforms like Amazon and Taobao rely on optimizing CTR and CVR estimation to boost gross merchandise volume (GMV), while advertising platforms at Google and Meta depend on it to drive revenue growth. In the past decade, as deep learning has been widely adopted in ASR applications, most estimation models have been built on deep learning frameworks and rely on large-scale, sparse categorical features (Cheng et al. (2016); Guo et al. (2017); Lian et al. (2018)). Recent work (Zhang et al. (2022b)) demonstrates, through extensive experiments, that such models commonly suffer from the one-epoch overfitting phenomenon, where model performance drops sharply after the first epoch of training. It empirically suggests that the optimal practice is to train the models for only one epoch. At the same time, their empirical analysis also reveals a strong connection between feature sparsity and the one-epoch phenomenon. In ASR scenarios, categorical features can easily reach the scale of billions, and most feature values occur extremely infrequently (Xie et al. (2020); Zhang et al. (2022a)), which makes models especially susceptible to overfitting after the first epoch. Additionally, Ouyang et al. (2022) reported a similar one-epoch phenomenon during supervised fine-tuning (SFT) of large language model (LLM), though they argue that moderate overfitting can actually be beneficial. We leave it in future work. In this paper, we focus on addressing the multi-epoch overfitting problem for models with large-scale sparse features in ASR applications.

Liu et al. (2023) was the first to address the one-epoch problem using a heuristic approach. They introduced a multi-epoch data augmentation method (MEDA) that can be easily applied to estimation models with large-scale sparse categorical features. Later, they extended it to a continual learning paradigm (Fan et al. (2024)). To mitigate overfitting during multi-epoch training, MEDA reinitializes the embeddings of categorical features and their corresponding optimizer states at the beginning of each epoch. Although this approach effectively alleviates multi-epoch overfitting, it is fundamentally heuristic because the embedding parameters are only reinitialized at epoch boundaries. It neither ensures optimal convergence nor explains the root cause of overfitting. Moreover,

---

\*Equal contribution.

this embedding reinitialization approach may result in the loss of substantial information, potentially resulting in suboptimal model performance. Nevertheless, it provides important inspiration for subsequent research. Another method, proposed by Wang et al. (2025), adopts an LLM-style paradigm. In this approach, generative pretraining is used to obtain embeddings for categorical features, which remain frozen during subsequent training. This strategy also helps to mitigate overfitting. However, it requires significant training resources to obtain the pretrained embeddings, and the performance cannot be fairly compared to single-epoch training because the parameter budget used during the pretraining phase is not included. Therefore, it cannot be regarded as a solution to the one-epoch problem, although it does highlight the pivotal role of the embedding layer in this phenomenon.

There are several well-established and general-purpose methods to mitigate overfitting, such as dropout (Srivastava et al. (2014)),  $L_1$  and  $L_2$  regularization (Schmidt et al. (2009); Moore & DeNero (2011)), and weight decay (Hanson & Pratt (1988)). However, in real-world industrial applications, data is typically high-dimensional and sparse, with different features exhibiting varying degrees of sparsity. Consequently, methods like AdamW (Loshchilov & Hutter (2017)), which apply the same weight decay across all parameters, tend to be suboptimal for addressing overfitting. Specifically, such approaches may reduce the fitting accuracy for relatively dense features while failing to effectively control overfitting in sparse features.

This paper presents a foundational theoretical analysis of the root cause of one-epoch overfitting, and proposes a method that adaptively determines regularization coefficients according to the effective update interval of each categorical feature value, and integrates these coefficients into the optimizer’s update rules. The proposed approach is particularly well-suited for models with large-scale sparse features. It reduces regularization for relatively dense features and neural network parameters, while assigning appropriate regularization strengths to individual categorical features. As a result, this method not only prevents the sharp performance degradation observed in multi-epoch training, but also enhances performance within a single epoch.

## 2 PRELIMINARY

In the industrial ASR domain, mainstream estimation models typically combine embedding layers with a variety of dense multi-layer perceptron (MLP) backbones, such as Gu et al. (2022). Taking an e-commerce platform estimation model as an example, these models process large-scale sparse inputs, including item IDs, brand IDs, and seller IDs, where the scale of categorical features can range from millions to billions. Before being processed by the estimation model, these sparse features are first mapped to low-dimensional dense representations via embedding layers. The one-hot categorical feature  $\mathbf{x}_i(t) \in \mathbb{R}^{N_i}$  is defined as  $\mathbf{x}_i(t) = [0, 0, \dots, 1, \dots, 0]^\top$ ,  $i \in [S], t \in [T]$ , which can be represented by an embedding vector  $\mathbf{e}_i(t) \in \mathbb{R}^{d_i}$  shown below

$$\mathbf{e}_i(t) = \mathbf{E}_i^\top \mathbf{x}_i(t) \quad (1)$$

where  $\mathbf{E}_i \in \mathbb{R}^{N_i \times d_i}$  is the embedding matrix for feature  $i$  and  $d_i$  is the embedding size.  $T \in \mathbb{N}$  is the number of training samples.  $S \in \mathbb{N}$  denotes the number of categorical features.  $N_i \in \mathbb{N}, \forall i \in [S]$  denotes the number of distinct values for feature  $i$ . At each update step, an embedding lookup is performed to retrieve the dense representations for the sparse features via equation 1, which are then fed into the MLP layers. For simplicity, we separate the model into the embedding component and the MLP component denoted as  $f$ . In our theoretical analysis, we use a basic DNN backbone and provide experiments in section 4 to demonstrate the generalizability of our method with other backbone architectures.

### 2.1 NEURAL NETWORK DEFINITION

The general form of basic DNN function can be defined as

$$f(\cdot) = \mathbf{W}_L \sigma_{L-1}(\mathbf{W}_{L-1} \sigma_{L-2}(\dots \sigma_1(\mathbf{W}_1 \cdot))) \quad (2)$$

where  $L$  denotes the number of MLP layers,  $\sigma(\cdot)$  is the ReLU function (Agarap (2018)),  $\mathbf{W}_l$  is the linear projection matrix of layer  $l, l \in [L]$ . In this paper, we only discuss the impact of embedding layer so we can define the  $t$ -th sample output of DNN as

$$\mathbf{y}(t) = f([\mathbf{E}_1^\top \mathbf{x}_1(t); \mathbf{E}_2^\top \mathbf{x}_2(t); \dots; \mathbf{E}_S^\top \mathbf{x}_S(t)]) \quad (3)$$

where  $\mathbf{y}(t)$  is the logit output for CTR or CVR estimation model.

## 2.2 RADEMACHER COMPLEXITY BOUND

Rademacher complexity is a standard tool to control the uniform convergence of given classes of predictors (Koltchinskii & Panchenko (2002), Zhang et al. (2016)). Formally, given a real-valued function class  $\mathcal{H}$  with the input  $\mathbf{z}$ , we define the empirical Rademacher complexity  $\widehat{\mathcal{R}}_T(\mathcal{H})$  as

$$\widehat{\mathcal{R}}_T(\mathcal{H}) = \mathbb{E}_\epsilon \left[ \sup_{h \in \mathcal{H}} \frac{1}{T} \sum_{t=1}^T \epsilon_t h(\mathbf{z}_t) \right] \quad (4)$$

where  $\epsilon = (\epsilon_1, \dots, \epsilon_T)$  is a vector whose entries  $\epsilon_t$  are independent and uniformly distributed in  $\{-1, +1\}$ . Using standard arguments, such bounds, as long as the norm of  $\mathbf{z}_t$  is bounded, can be converted to bounds on the generalization error, assuming access to a sample of  $T$  i.i.d. training samples.

Based on Theorem 1 of Golowich et al. (2018), and noting that the embedding layer can be regarded as a linear projection, we can obtain the following upper bound on the Rademacher complexity of equation 3 as

$$\widehat{\mathcal{R}}_T(\mathcal{H}_L) \leq \frac{1}{T} \left( \prod_{l=1}^L M_F(l) \right) \left( \sqrt{\sum_{i=1}^S M_{E_i}^2} \right) \left( \sqrt{2 \log(2)L} + 1 \right) \sqrt{\sum_{t=1}^T \sum_{i=1}^S \|\mathbf{x}_i(t)\|^2} \quad (5)$$

where  $\|\cdot\|$  denotes  $\ell_2$  norm, and each matrix  $\mathbf{W}_l$  in function  $f$  has Frobenius norm at most  $M_F(l)$ ,  $l \in [L]$ .  $M_{E_i}$  is the Frobenius norm of embedding matrix  $\mathbf{E}_i$  and the activation functions are assumed to be 1-Lipschitz and positive-homogeneous. Furthermore, this upper bound can be rewritten as

$$\widehat{\mathcal{R}}_T(\mathcal{H}_L) \leq \frac{\left( \prod_{l=1}^L M_F(l) \right) \sqrt{S}}{\sqrt{T}} \left( \sqrt{\sum_{i=1}^S \sum_{j=1}^{N_i} \tau_{ij}} \right) \left( \sqrt{2 \log(2)L} + 1 \right) \quad (6)$$

where  $\tau_{ij}$  is the squared  $\ell_2$  norm of  $j$ -th row of embedding matrix  $\mathbf{E}_i$ . In ASR applications, the majority of parameters are concentrated in the embedding layers. Thus, we can see that  $\sum_{i=1}^S \sum_{j=1}^{N_i} \tau_{ij}$  has a significant impact on the upper bound of Rademacher complexity, and consequently, on the generalization error bound.

## 3 THE PROPOSED APPROACH

As discussed in section 2, high-dimensional embedding matrices lead to increased generalization error bounds if the training loss remains constant. On the other hand, strictly constraining the norms of the embedding vectors to reduce Rademacher complexity may increase the training error, thus potentially degrading overall performance. To identify the optimal regularization factor, we formulate this trade-off as a constrained optimization problem, described as follows.

$$\min_{\tau_{ij} > 0} \sum_{i=1}^S \sum_{j=1}^{N_i} m_{ij} \varphi(\tau_{ij}) \quad \text{s.t.} \quad \sum_{i=1}^S \sum_{j=1}^{N_i} \tau_{ij} \leq C \quad (7)$$

where  $\varphi(\tau_{ij}) = \min_{\|\mathbf{e}_{ij}\|^2 \leq \tau_{ij}} \mathcal{L}(\mathbf{e}_{ij})$  with  $i \in [S]$  and  $j \in [N_i]$ . Here,  $\mathbf{e}_{ij}$  denotes the  $j$ -th row of embedding matrix  $\mathbf{E}_i$ , and  $\mathcal{L}(\mathbf{e}_{ij})$  represents the average cross-entropy (CE) loss evaluated on the DNN output when the training sample activates  $\mathbf{e}_{ij}$ . For the CE loss function,  $\mathcal{L}(\mathbf{e}_{ij})$  is lower semi-continuous and bounded below on bounded sets (Goodfellow et al. (2016)). Consequently,  $\varphi(\tau_{ij})$  is well-defined (Ok (2011)) and monotonically non-increasing in  $\tau_{ij}$ , since the feasible set expands with  $\tau_{ij}$ . Here,  $\tau_{ij}$  is the squared norm budget of embedding vector  $\mathbf{e}_{ij}$ . According to DiBenedetto (2016),  $\varphi(\tau_{ij})$  is differentiable almost everywhere, and we assume that  $\varphi(\tau_{ij})$  is differentiable at the optimal points  $\tau_{ij}^*$  for analysis. The coefficient  $m_{ij}$  denotes the sample frequency with which embedding vector  $\mathbf{e}_{ij}$  appears in the training dataset and  $C$  is a constant that defines the global norm upper bound for embedding layers. As shown in equation 6, the value of  $C$  directly determines the Rademacher complexity upper bound.

**Proposition 1** A necessary condition for the optimal regularization multiplier  $\lambda_{ij}^*$  associated with the  $\|e_{ij}\|^2 \leq \tau_{ij}^*$  is given by  $\lambda_{ij}^* = \mu_0/m_{ij}$ , where  $\mu_0$  is the Lagrange multiplier corresponding to  $\sum_{i=1}^S \sum_{j=1}^{N_i} \tau_{ij}^* \leq C$ .

*Proof.* Based on the above assumption, at points of differentiability where a standard constraint qualification holds for the inner optimal solution, the envelope theorem and Lagrangian decomposition (Shapiro (1979)) yield

$$\varphi'(\tau_{ij}^*) = -\lambda_{ij}^* \quad (8)$$

where  $\lambda_{ij}^* \geq 0$  is the Lagrange multiplier corresponding to  $\|e_{ij}\|^2 \leq \tau_{ij}^*$ , and  $\tau_{ij}^*$  is the optimal solution of equation 7. Here,  $\varphi'(\tau_{ij}^*)$  denotes the derivative of  $\varphi(\tau_{ij}^*)$  with respect to  $\tau_{ij}^*$ . We reformulate the optimization problem defined in equation 7 with the Lagrange multipliers  $\mu_{ij}$  and  $\mu_0$ , corresponding to the nonnegativity constraints of  $\tau_{ij} \geq 0$  and  $\sum_{i=1}^S \sum_{j=1}^{N_i} \tau_{ij} \leq C$  respectively, where  $\mu_{ij}$  and  $\mu_0$  are restricted to be non-negative.

$$\begin{aligned} \min_{\tau_{ij} > 0} & \left( \sum_{i=1}^S \sum_{j=1}^{N_i} m_{ij} \varphi(\tau_{ij}) + \mu_0 \left( \sum_{i=1}^S \sum_{j=1}^{N_i} \tau_{ij} - C \right) - \sum_{i=1}^S \sum_{j=1}^{N_i} \mu_{ij} \tau_{ij} \right) \\ \text{s.t. } & \mu_0 \geq 0, \mu_{ij} \geq 0, \forall i \in [S], \forall j \in [N_i] \end{aligned} \quad (9)$$

Based on the KKT condition (Boyd & Vandenberghe (2004)), we have  $m_{ij}\varphi'(\tau_{ij}^*) + \mu_0 - \mu_{ij} = 0$ . Applying the complementary slackness condition, we obtain  $\mu_{ij}\tau_{ij}^* = 0$ . This implies the optimality condition for  $\tau_{ij} > 0$  can be simplified as

$$m_{ij}\varphi'(\tau_{ij}^*) + \mu_0 = 0 \quad (10)$$

By substituting equation 8 into equation 10, we obtain a necessary condition for the optimal regularization multiplier  $\lambda_{ij}^* = \mu_0/m_{ij}$ .

### 3.1 ADAPTIVE REGULARIZATION METHOD

As shown in equation 6, embedding layers in ASR applications typically take the majority of the model parameters and have a substantial impact on the generalization error bound. Proposition 1 suggests that the norm budget for each embedding vector should be allocated according to its sample frequency. However, it is not easy to use the frequency directly during the training process. We can estimate  $m_{ij}$  via the stochastic occurrence interval  $I_{ij}$  of  $e_{ij}$  for  $i \in [S]$  and  $j \in [N_i]$ . Specifically, given that  $\mathbf{x}_i(t)$  is sampled from an i.i.d. distribution (a common assumption in deep learning), we have  $\mathbb{E}[m_{ij}] = T/\mathbb{E}[I_{ij}]$  (Papoulis (1965)). It enables us to incorporate frequency estimation into the norm budget allocation strategy during training.

Based on the analysis above, we propose an adaptive method that assigns the regularization strength based on the occurrence interval of each embedding vector. Specifically, at each training step  $k$ , we define last valid update step (LVS) for the embedding vector  $e_{ij}$  as  $s_{ij}$ . If the gradient norm of  $e_{ij}$  satisfies  $\|\mathbf{g}_{ij}\| > 0$ , we update the LVS by setting  $s_{ij} = k$ . Otherwise,  $s_{ij}$  retains its previous value. Therefore,  $s_{ij}$  serves as a lazy-update variable. We define the stochastic update interval as  $I_{ij} = k - s_{ij} - 1$ . The feature-wise regularization coefficient  $\lambda_{ij}$  is then dynamically computed as below

$$\lambda_{ij} = \min(1, \alpha I_{ij}), i \in [S], j \in [N_i] \quad (11)$$

Here,  $\alpha \in [0, 1)$  denotes the base regularization coefficient. Following the decoupled weight decay approach in AdamW (Loshchilov & Hutter (2017)), we incorporate the dynamically computed regularization into each optimizer update step. Algorithm 1 outlines the procedure of Adam with adaptive regularization (AdamAR).

For clarity and practical implementation, we use  $\theta_p$  to denote parameters in the estimation model, where  $p \in [P]$  and  $P$  is the total number of parameters. At each update step  $k$ , we first compute the adaptive regularization  $\lambda_p^k$  according to equation 11 and use it to update the corresponding model parameter  $\theta_p^k$ . We then identify the parameters whose gradient norm  $\|\mathbf{g}_p^k\|$  is greater than zero in current step and update their last update step state  $s_p^k$  for use in the next iteration.

In fact, our method is not only suitable for Adam, but also compatible with various gradient-based optimizers which have weight decay factor, such as Adagrad (Duchi et al. (2011)). We have implemented an adaptive version for Adagrad in algorithm 2 of the appendix B. In section 4, we conducted comparative experiments evaluating performance across both Adam and Adagrad.

---

**Algorithm 1** Adam with Adaptive Regularization (AdamAR)

---

- 1: given  $\beta_1 = 0.9, \beta_2 = 0.999, \varepsilon = 10^{-8}, \alpha$ , learning rate  $\eta$
  - 2: initialize time step  $k \leftarrow 0$ , parameter  $\theta_p^{k=0}$ , first moment  $m_p^{k=0} \leftarrow 0$ , second moment  $v_p^{k=0} \leftarrow 0$ , last update step state  $s_p^{k=0} \leftarrow 0$
  - 3: **repeat**
  - 4:    $k \leftarrow k + 1$
  - 5:    $g_p^k \leftarrow \nabla_{\theta_p} f(\theta_p^{k-1})$  (Get gradients w.r.t. stochastic objective at timestep  $t$ )
  - 6:    $m_p^k \leftarrow \beta_1 m_p^{k-1} + (1 - \beta_1) g_p^k$  (Update biased first moment estimate)
  - 7:    $v_p^k \leftarrow \beta_2 v_p^{k-1} + (1 - \beta_2) (g_p^k)^2$  (Update biased second raw moment estimate)
  - 8:    $\hat{m}_p^k \leftarrow m_p^k / (1 - \beta_1^k)$  (Compute bias-corrected first moment estimate)
  - 9:    $\hat{v}_p^k \leftarrow v_p^k / (1 - \beta_2^k)$  (Compute bias-corrected second raw moment estimate)
  - 10:    $\lambda_p^k \leftarrow \min(1, (k - s_p^{k-1} - 1) \alpha)$  (Compute adaptive regularization through equation 11)
  - 11:    $s_p^k \leftarrow k$  if  $\|g_p^k\| > 0$  else  $s_p^{k-1}$  (Update the last update step when the gradient norm is greater than zero)
  - 12:    $\theta_p^k \leftarrow \theta_p^{k-1} - \lambda_p^k \theta_p^{k-1} - \eta \cdot \hat{m}_p^k / (\sqrt{\hat{v}_p^k} + \varepsilon)$  (Update parameters)
  - 13: **until** stopping criterion is met
  - 14: return optimized parameters  $\theta_p^t$
- 

### 3.2 DISCUSSION ON THE MECHANISM OF REGULARIZATION

As shown in equation 7, if we do not constrain the embedding norm, the global norm will continue to grow until further increases no longer yield improvements in the objective value since  $\varphi(\tau_{ij})$  is non-increasing. In other words, the embedding norms will continue to grow during training, resulting in a looser upper bound on the Rademacher complexity. The sharper drop in performance during multi-epoch training can be attributable to the increased Rademacher complexity resulting from unconstrained norm growth as demonstrated in the experimental section 4.4.

Then we discuss how the adaptive regularization takes effect, and also provides guidance for selecting the regularization coefficient  $\alpha$ .

**Proposition 2** *When adaptive regularization is applied according to equation 11, the update rule for parameters satisfy  $\|\theta_p^{k-1} - \lambda_p^k \theta_p^{k-1} - \eta \cdot \hat{m}_p^k / (\sqrt{\hat{v}_p^k} + \varepsilon)\| \leq (1 - \alpha)^{I_p^k} \|\theta_p^{k-1}\| + \|\eta \cdot \hat{m}_p^k / (\sqrt{\hat{v}_p^k} + \varepsilon)\|$*

*Proof.* Let  $I_p^k \in \mathbb{Z}_{\geq 0} \cap [0, 1/\alpha)$ , and  $\alpha$  is typically chosen such that  $\alpha \in [0, 1)$ . By applying Bernoulli's inequality to  $(1 - \alpha)^{I_p^k}$ , we obtain  $(1 - \alpha)^{I_p^k} \geq 1 - \alpha I_p^k$ . In the case where  $I_p^k \in \mathbb{Z}_{\geq 0} \cap [1/\alpha, \infty)$ , it follows that  $(1 - \alpha)^{I_p^k} > 0$  since  $\alpha < 1$  and  $I_p^k \geq 0$ . Combining both cases, we have

$$(1 - \alpha)^{I_p^k} \geq 1 - \min(1, \alpha I_p^k) \quad (12)$$

We substitute equation 12 into  $\theta_p^{k-1} - \lambda_p^k \theta_p^{k-1} - \eta \cdot \hat{m}_p^k / (\sqrt{\hat{v}_p^k} + \varepsilon)$ , then we can have

$$\|\theta_p^{k-1} - \lambda_p^k \theta_p^{k-1} - \eta \cdot \hat{m}_p^k / (\sqrt{\hat{v}_p^k} + \varepsilon)\| \leq (1 - \alpha)^{I_p^k} \|\theta_p^{k-1}\| + \|\eta \cdot \hat{m}_p^k / (\sqrt{\hat{v}_p^k} + \varepsilon)\| \quad (13)$$

From proposition 2, the update rule for  $\theta_p^k$  can be interpreted intuitively. If the interval  $I_p^k$  is large for the corresponding sparse categorical features, the term  $(1 - \alpha)^{I_p^k} \|\theta_p^{k-1}\|$  becomes negligible, and  $\theta_p^k$  is effectively determined by the latest gradient. In the ASR domain, certain categorical feature values may not appear in every mini-batch, resulting in their embedding parameters being updated

infrequently, while the MLP parameters are updated in every batch. After the MLP component has nearly converged, the embedding parameters associated with sparse features will have received far fewer updates and may become misaligned with the current state of the MLP parameters, making the previous value  $\theta_p^{k-1}$  less informative. Proposition 2 demonstrates that the factor  $(1 - \alpha)^{I_p^k}$  exponentially attenuates the previous value  $\theta_p^{k-1}$ , making the embedding parameters of sparse features depend more heavily on the current gradient. Meanwhile, since the update interval  $I_p^k$  for MLP parameters is identically zero (as they are updated in every batch), the regularization primarily affects the embedding parameters corresponding to very low-frequency feature values.

Moreover, we observe that the method proposed in Liu et al. (2023) is a special case of our approach when zero reinitialization is applied to the embedding and  $I_p^k$  is specified as

$$I_p^k = \begin{cases} 1/\alpha, & \text{if } kB \bmod T = 0 \\ 0, & \text{otherwise} \end{cases} \quad (14)$$

Where  $B$  is the batch size. It can be seen that this heuristic is primarily effective at epoch boundaries. However, for features that have already become overfitted within a single epoch, its performance remains suboptimal.

## 4 EXPERIMENTAL VALIDATION

To evaluate the effectiveness of our proposed method, we conduct several experiments on different public datasets and our industrial dataset. The experimental setup is described in section 4.1. The training framework proposed by Zhu et al. (2022) is used for training on public datasets, while XDL (Jiang et al. (2019)) is employed for training our proprietary industrial dataset. We show the learning curve on the Avazu dataset in section 4.2 to demonstrate the better generalization of our methods over multi-epoch training. In section 4.3, we compare multiple backbones and datasets to prove the generalization of our method. Finally, we give a detailed example to show that the low-frequency embeddings are the primary contributors of one-epoch problem, which demonstrates we should allocate a smaller norm budget to embeddings with lower sample frequency. For reproduction, the code<sup>1</sup> is available.

### 4.1 EXPERIMENTAL SETUP

#### 4.1.1 DATASETS

In our experiments, we use three public datasets as well as an online business dataset from sponsored search. Details of these datasets are provided below.

**iPinYou**<sup>2</sup>. The training dataset includes processed bidding, impression, click, and conversion logs from iPinYou DSP. It contains 19.5 million records and 16 categorical features, providing a suitable context for exemplifying the overfitting phenomenon.

**Amazon**<sup>3</sup>. This is a widely used dataset from Amazon for evaluating CTR estimation models. In our study, we use the electronics category of the Amazon dataset, which contains approximately 3 million records and 3 categorical features. Popular models such as DIN (Zhou et al. (2018)) has used this dataset for performance evaluation.

**Avazu**<sup>4</sup>. This dataset comprises approximately 10 days of labeled click-through data from mobile advertisements, consisting of 40 million records and 22 categorical features spanning both user attributes and advertisement characteristics. Many of these features are highly dimensional, making this dataset a common benchmark for CTR estimation.

**LZD**. The dataset is sampled from our production environment and consists of real-time bidding logs from sponsored search. The dataset contains 25 million records and 13 categorical features.

<sup>1</sup><https://anonymous.4open.science/r/AdaptiveRegularization-AIDC/>

<sup>2</sup>[https://huggingface.co/datasets/reczoo/iPinYou\\_x1](https://huggingface.co/datasets/reczoo/iPinYou_x1)

<sup>3</sup>[https://huggingface.co/datasets/reczoo/AmazonElectronics\\_x1](https://huggingface.co/datasets/reczoo/AmazonElectronics_x1)

<sup>4</sup>[https://huggingface.co/datasets/reczoo/Avazu\\_x1](https://huggingface.co/datasets/reczoo/Avazu_x1)

---

#### 4.1.2 MLP BACKBONE

We test our method with four backbones as follows:

**DNN.** It is a basic deep learning model defined in equation 2.

**WDL** (Cheng et al. (2016)). It combines a linear model and a deep neural network to capture both memorization and generalization for recommender systems.

**DeepFM** (Guo et al. (2017)). It integrates factorization machines for learning low-order feature interactions and deep neural networks for high-order feature interactions.

**WuKong** (Gu et al. (2022)). It proposes a specific model designed to explore these scaling laws. Its architecture is constructed with deeper and wider layers to capture high-order feature interactions.

#### 4.1.3 METHODS AND HYPERPARAMETERS

To evaluate the one-epoch overfitting phenomenon, we set the number of training epochs to 4 and compare the performance of four benchmarks as follows:

**Baseline optimizer.** Adam and Adagrad serve as the baseline optimizers.

**MEDA.** MEDA is applied using the same optimizer settings as in baseline.

**AdamW and AdagradW.** The baseline optimizers are enhanced with weight decay.

**AdamAR and AdagradAR.** The baseline optimizers are combined with our method.

The hyperparameter settings are as follows. The embedding dimension is set to 32, with zero initialization. The learning rate is set to 0.001 for Adam and 0.01 for Adagrad, respectively. The batch size is 2048. Both  $\alpha$  and the weight decay parameter are selected via grid search over the range  $10^{-7}$  to  $10^{-1}$ , with the best hyperparameter settings determined according to validation performance (see appendix D for details). Network architectures are configured with minor adjustments across datasets. For detailed configurations, please refer to table 3 in appendix C. All other hyperparameters are set to their default values. Area under the curve (AUC) and binary cross-entropy loss are used as evaluation metrics. Experiments are conducted on a single machine with an NVIDIA L20 GPU.

## 4.2 LEARNING CURVE AND GENERALIZATION RESULTS

In this section, we present the training loss and test AUC across multiple epochs on the Avazu dataset, using a DNN backbone and the Adam optimizer. The learning curves in figure 1 compare our method with several baselines. For the native optimizer, training loss decreases rapidly after the first epoch. However, test AUC drops sharply with additional epochs, indicating clear overfitting. In contrast, MEDA and weight decay alleviate this problem, yielding more stable test AUC throughout training. Our method achieves the best overall performance. Figures 1(b) and 1(c) reveal an inverse correlation between the  $\ell_2$  norm of the embedding vectors and test AUC. It demonstrates that constraining the embedding norm improves generalization ability of models. Among all methods, our proposed AdamAR achieves the lowest cumulative  $\ell_2$  norm for the embedding vectors, highlighting its effectiveness in controlling regularization strength.

## 4.3 PERFORMANCE OVER DIFFERENT DATASETS AND MLP BACKBONES

In this section, we compare test AUC across different datasets and MLP backbones to demonstrate the generalization capability of our method. The results, summarized in table 1 and table 2, show that our methods consistently outperform other approaches on all datasets and architectures, achieving superior AUC in both single-epoch and multi-epoch training. Furthermore, the gains are consistent across diverse model architectures, ranging from basic DNN to more sophisticated designs like WuKong, which capture complex feature interactions. Overall, these results demonstrate the robustness and versatility of our adaptive regularization approach across various settings.

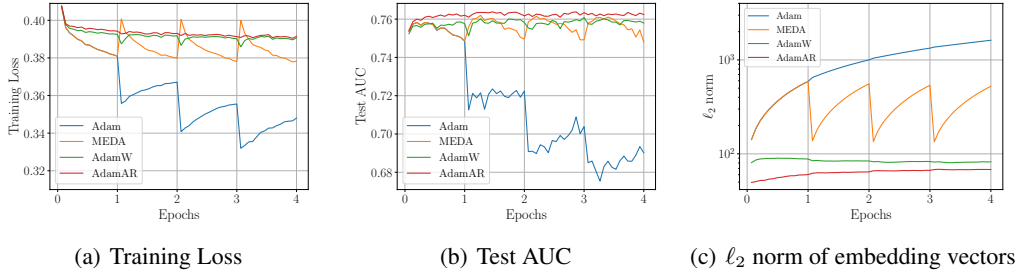


Figure 1: Performance of four methods on Avazu dataset with DNN backbone. (a) shows the training loss curves. (b) presents the test AUC. (c) illustrates the cumulative  $\ell_2$  norm of embedding vectors.

Table 1: Comparison of test AUC across different datasets and models with the Adam optimizer. E1-E4 denote results after 1-4 epochs, respectively. The best results are highlighted in bold.

Dataset	Method	DNN				WDL				DeepFM				WuKong			
		E1	E2	E3	E4												
iPinYou	Adam	0.7498	0.7258	0.7174	0.7026	0.7622	0.7322	0.6972	0.6978	0.7595	0.7343	0.7057	0.6983	0.7644	0.7437	0.7137	0.6955
	MEDA	0.7498	0.7631	0.7713	0.7692	0.7622	0.7582	0.7574	0.7506	0.7595	0.7582	0.7546	0.7518	0.7644	0.7671	0.7686	0.7714
	AdamW	0.7486	0.7595	0.7628	0.7500	0.7609	0.7615	0.7692	0.7644	0.7600	0.7584	0.7486	0.7367	0.7593	0.7687	0.7586	0.7549
	AdamAR	<b>0.7549</b>	<b>0.7728</b>	<b>0.7730</b>	<b>0.7725</b>	<b>0.7675</b>	<b>0.7701</b>	<b>0.7692</b>	<b>0.7650</b>	<b>0.7677</b>	<b>0.7683</b>	<b>0.7637</b>	<b>0.7590</b>	<b>0.7668</b>	<b>0.7737</b>	<b>0.7722</b>	<b>0.7738</b>
Amazon	Adam	0.8482	0.8532	0.8314	0.8179	0.8489	0.8500	0.8255	0.8123	0.8496	0.8510	0.8236	0.8117	0.8574	0.8577	0.8355	0.8219
	MEDA	0.8482	0.8537	0.8561	0.8574	0.8489	0.8506	0.8565	0.8557	0.8496	0.8511	0.8560	0.8557	0.8574	0.8577	0.8601	0.8627
	AdamW	0.8472	0.8554	0.8409	0.8268	0.8473	0.8524	0.8377	0.8195	0.8472	0.8523	0.8380	0.8192	0.8544	0.8615	0.8442	0.8315
	AdamAR	<b>0.8506</b>	<b>0.8669</b>	<b>0.8709</b>	<b>0.8683</b>	<b>0.8513</b>	<b>0.8656</b>	<b>0.8690</b>	<b>0.8645</b>	<b>0.8513</b>	<b>0.8657</b>	<b>0.8690</b>	<b>0.8644</b>	<b>0.8576</b>	<b>0.8687</b>	<b>0.8702</b>	<b>0.8664</b>
Avazu	Adam	0.7483	0.7229	0.6973	0.6868	0.7485	0.7226	0.6949	0.6895	0.7488	0.7196	0.6918	0.6821	0.7479	0.7322	0.7000	0.7147
	MEDA	0.7483	0.7508	0.7479	0.7479	0.7485	0.7475	0.7472	0.7516	0.7488	0.7478	0.7441	0.7523	0.7479	0.7538	0.7555	0.7559
	AdamW	0.7584	0.7594	0.7579	0.7576	0.7586	0.7590	0.7544	0.7580	0.7590	0.7586	0.7546	0.7580	0.7511	0.7533	0.7565	0.7553
	AdamAR	<b>0.7621</b>	<b>0.7640</b>	<b>0.7636</b>	<b>0.7625</b>	<b>0.7630</b>	<b>0.7622</b>	<b>0.7617</b>	<b>0.7630</b>	<b>0.7629</b>	<b>0.7623</b>	<b>0.7613</b>	<b>0.7636</b>	<b>0.7619</b>	<b>0.7607</b>	<b>0.7624</b>	<b>0.7620</b>
LZD	Adam	0.7148	0.6661	0.6250	0.6105	0.7147	0.6719	0.6305	0.6053	0.7131	0.6706	0.6237	0.6105	0.7156	0.6629	0.6165	0.6069
	MEDA	0.7148	0.7110	0.7113	0.7177	0.7147	0.7183	0.7169	0.7157	0.7131	0.7125	0.7157	0.7149	0.7156	0.7181	0.7182	0.7185
	AdamW	0.7146	0.7132	0.7107	0.7138	0.7142	0.7136	0.7143	0.7129	0.7121	0.7107	0.7140	0.7132	0.7126	0.7149	0.7163	0.7115
	AdamAR	<b>0.7238</b>	<b>0.7256</b>	<b>0.7238</b>	<b>0.7234</b>	<b>0.7226</b>	<b>0.7233</b>	<b>0.7236</b>	<b>0.7242</b>	<b>0.7227</b>	<b>0.7199</b>	<b>0.7218</b>	<b>0.7221</b>	<b>0.7239</b>	<b>0.7218</b>	<b>0.7201</b>	<b>0.7185</b>

#### 4.4 EXAMPLE OF THE ROOT CAUSE OF OVERFITTING

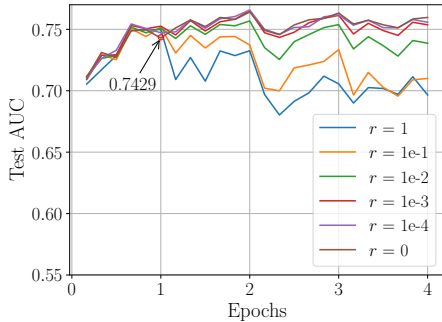
In this section, we give an example to show the root cause of multi-epoch overfitting. We use the iPinYou dataset with DNN backbone and Adam to illustrate this issue. The detailed feature statistics are listed in table 4 in appendix E. We can observe that most features on iPinYou dataset are relatively dense, and their mean update intervals during training are less than 1. To investigate the root cause of overfitting, we select the feature "IP", which is the most sparse feature in iPinYou dataset with 704,966 unique IDs. We apply a filtering procedure to reduce its feature sparsity. Given a ratio  $r$ , we only retain the top- $r$  fraction (by frequency) of IDs and replace other IDs with a default ID.

Figure 2(a) demonstrates that as  $r$  decreases, the test AUC remains stable across multiple epochs, indicating that the one-epoch overfitting phenomenon is effectively alleviated. It suggests that low-frequency IDs in the "IP" feature are the primary cause of one-epoch overfitting in the iPinYou dataset. Based on this observation, a straightforward approach to mitigate this issue is to exclude the "IP" feature. However, as shown by the case  $r = 0$ , removing the "IP" feature results in a substantial test AUC drop (from 0.7498 to 0.7429) at the end of the first epoch.

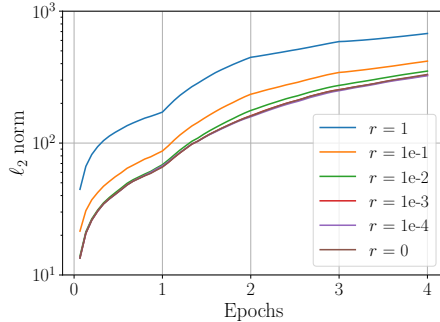
Although removing sparse features can mitigate the one-epoch overfitting issue, it often leads to diminished model performance. In contrast, our proposed method dynamically adjusts the regularization strength, effectively preventing overfitting while maintaining strong predictive performance.

Table 2: Comparison of test AUC across different datasets and models with the Adagrad optimizer. E1-E4 denote results after 1-4 epochs, respectively. The best results are highlighted in bold.

Dataset	Method	DNN				WDL				DeepFM				WuKong			
		E1	E2	E3	E4												
iPinYou	Adagrad	0.7626	0.6496	0.6366	0.6079	0.7623	0.6697	0.6424	0.6190	0.7626	0.6745	0.6440	0.6202	0.7651	0.6962	0.6489	0.5994
	MEDA	0.7626	0.7673	0.7733	0.7689	0.7623	0.7725	0.7650	0.7717	0.7626	0.7722	0.7660	0.7728	0.7651	0.7756	0.7730	0.7712
	AdagradW	0.7586	0.7614	0.7651	0.7570	0.7538	0.7652	0.7656	0.7598	0.7511	0.7662	0.7631	0.7632	0.7544	0.7704	0.7657	0.7645
	AdagradAR	<b>0.7717</b>	<b>0.7706</b>	<b>0.7759</b>	<b>0.7709</b>	<b>0.7705</b>	<b>0.7763</b>	<b>0.7758</b>	<b>0.7725</b>	<b>0.7703</b>	<b>0.7767</b>	<b>0.7741</b>	<b>0.7739</b>	<b>0.7689</b>	<b>0.7803</b>	<b>0.7792</b>	<b>0.7774</b>
Amazon	Adagrad	0.8435	0.8392	0.8127	0.8019	0.8427	0.8359	0.8113	0.7985	0.8425	0.8359	0.8102	0.8005	0.8487	0.8465	0.8176	0.8050
	MEDA	0.8435	0.8477	0.8506	0.8521	0.8427	0.8480	0.8500	0.8503	0.8425	0.8493	0.8471	0.8522	0.8487	0.8568	0.8584	0.8613
	AdagradW	0.8429	0.8564	0.8553	0.8533	0.8432	0.8554	0.8531	0.8492	0.8436	0.8556	0.8533	0.8492	0.8513	0.8616	0.8590	0.8584
	AdagradAR	<b>0.8474</b>	<b>0.8652</b>	<b>0.8709</b>	<b>0.8716</b>	<b>0.8462</b>	<b>0.8641</b>	<b>0.8696</b>	<b>0.8704</b>	<b>0.8462</b>	<b>0.8645</b>	<b>0.8697</b>	<b>0.8707</b>	<b>0.8539</b>	<b>0.8675</b>	<b>0.8708</b>	<b>0.8697</b>
Avazu	Adagrad	0.7547	0.7324	0.7154	0.7082	0.7555	0.7321	0.7175	0.7080	0.7553	0.7317	0.7165	0.7070	0.7531	0.7324	0.7170	0.7039
	MEDA	0.7547	0.7544	0.7532	0.7548	0.7555	0.7547	0.7544	0.7556	0.7553	0.7545	0.7545	0.7550	0.7531	0.7543	0.7561	0.7547
	AdagradW	0.7579	0.7586	0.7569	0.7563	0.7588	0.7572	0.7573	0.7593	0.7592	0.7586	0.7570	0.7586	0.7482	0.7554	0.7549	0.7551
	AdagradAR	<b>0.7626</b>	<b>0.7629</b>	<b>0.7629</b>	<b>0.7622</b>	<b>0.7629</b>	<b>0.7640</b>	<b>0.7632</b>	<b>0.7634</b>	<b>0.7628</b>	<b>0.7633</b>	<b>0.7626</b>	<b>0.7620</b>	<b>0.7621</b>	<b>0.7617</b>	<b>0.7620</b>	<b>0.7612</b>
LZD	Adagrad	0.7232	0.6666	0.6417	0.6400	0.7252	0.6696	0.6374	0.6388	0.7254	0.6677	0.6409	0.6399	0.7280	0.6753	0.6449	0.6365
	MEDA	0.7232	0.7206	0.7137	0.7237	0.7252	0.7241	0.7253	0.7202	0.7254	0.7256	0.7245	0.7223	0.7280	0.7254	0.7252	0.7213
	AdagradW	0.7190	0.7057	0.7071	0.7119	0.7210	0.7139	0.7142	0.7100	0.7209	0.7110	0.7098	0.7105	0.7179	0.7076	0.6834	0.6869
	AdagradAR	<b>0.7232</b>	<b>0.7261</b>	<b>0.7204</b>	<b>0.7265</b>	<b>0.7284</b>	<b>0.7261</b>	<b>0.7256</b>	<b>0.7269</b>	<b>0.7280</b>	<b>0.7267</b>	<b>0.7258</b>	<b>0.7263</b>	<b>0.7281</b>	<b>0.7258</b>	<b>0.7254</b>	<b>0.7213</b>



(a) Test AUC



(b)  $\ell_2$  norm of embedding vectors

Figure 2: Performance comparison using various filter ratios for the "IP" feature on the iPinYou dataset. (a) shows the test AUC results. (b) presents the cumulative  $\ell_2$  norm of embedding vectors.

## 5 CONCLUSION

We propose an adaptive regularization method to address the one-epoch problem in estimation models for the ASR domain. Experimental results demonstrate that our approach effectively mitigates the one-epoch issue and improves estimation performance. Additionally, we provide a theoretical explanation for the one-epoch phenomenon and illustrate how the proposed method takes effect through analytical derivations and experiments. This approach has already been fully deployed in the production environment of sponsored search in our company.

## REFERENCES

- Abien Fred Agarap. Deep learning using rectified linear units (relu). *arXiv preprint arXiv:1803.08375*, 2018.
- Stephen P Boyd and Lieven Vandenberghe. *Convex optimization*. Cambridge university press, 2004.
- Heng-Tze Cheng, Levent Koc, Jeremiah Harmsen, Tal Shaked, Tushar Chandra, Hrishi Aradhye, Glen Anderson, Greg Corrado, Wei Chai, Mustafa Ispir, et al. Wide & deep learning for recommender systems. In *Proceedings of the 1st workshop on deep learning for recommender systems*, pp. 7–10, 2016.

- 
- Emmanuele DiBenedetto. *Real analysis*. Springer, 2016.
- John Duchi, Elad Hazan, and Yoram Singer. Adaptive subgradient methods for online learning and stochastic optimization. *Journal of machine learning research*, 12(7), 2011.
- Zhongxiang Fan, Zhaocheng Liu, Jian Liang, Dongying Kong, Han Li, Peng Jiang, Shuang Li, and Kun Gai. Multi-epoch learning with data augmentation for deep click-through rate prediction. *arXiv preprint arXiv:2407.01607*, 2024.
- Noah Golowich, Alexander Rakhlin, and Ohad Shamir. Size-independent sample complexity of neural networks. In *Conference On Learning Theory*, pp. 297–299. PMLR, 2018.
- Ian Goodfellow, Yoshua Bengio, Aaron Courville, and Yoshua Bengio. *Deep learning*, volume 1. MIT press Cambridge, 2016.
- Jiaxi Gu, Xiaojun Meng, Guansong Lu, Lu Hou, Niu Minzhe, Xiaodan Liang, Lewei Yao, Runhui Huang, Wei Zhang, Xin Jiang, et al. Wukong: A 100 million large-scale chinese cross-modal pre-training benchmark. *Advances in Neural Information Processing Systems*, 35:26418–26431, 2022.
- Huifeng Guo, Ruiming Tang, Yunming Ye, Zhenguo Li, and Xiuqiang He. Deepfm: a factorization-machine based neural network for ctr prediction. *arXiv preprint arXiv:1703.04247*, 2017.
- Stephen Hanson and Lorien Pratt. Comparing biases for minimal network construction with back-propagation. *Advances in neural information processing systems*, 1, 1988.
- Biye Jiang, Chao Deng, Huimin Yi, Zelin Hu, Guorui Zhou, Yang Zheng, Sui Huang, Xinyang Guo, Dongyue Wang, Yue Song, et al. Xdl: an industrial deep learning framework for high-dimensional sparse data. In *Proceedings of the 1st International Workshop on Deep Learning Practice for High-Dimensional Sparse Data*, pp. 1–9, 2019.
- Vladimir Koltchinskii and Dmitry Panchenko. Empirical margin distributions and bounding the generalization error of combined classifiers. *The Annals of Statistics*, 30(1):1–50, 2002.
- Jianxun Lian, Xiaohuan Zhou, Fuzheng Zhang, Zhongxia Chen, Xing Xie, and Guangzhong Sun. xdeepfm: Combining explicit and implicit feature interactions for recommender systems. In *Proceedings of the 24th ACM SIGKDD international conference on knowledge discovery & data mining*, pp. 1754–1763, 2018.
- Zhaocheng Liu, Zhongxiang Fan, Jian Liang, Dongying Kong, and Han Li. Multi-epoch learning for deep click-through rate prediction models. *arXiv preprint arXiv:2305.19531*, 2023.
- Ilya Loshchilov and Frank Hutter. Decoupled weight decay regularization. *arXiv preprint arXiv:1711.05101*, 2017.
- Robert Moore and John DeNero. L1 and l2 regularization for multiclass hinge loss models. In *MLSLP*, pp. 1–5, 2011.
- Efe A Ok. *Real analysis with economic applications*. Princeton University Press, 2011.
- Long Ouyang, Jeffrey Wu, Xu Jiang, Diogo Almeida, Carroll Wainwright, Pamela Mishkin, Chong Zhang, Sandhini Agarwal, Katarina Slama, Alex Ray, et al. Training language models to follow instructions with human feedback. *Advances in neural information processing systems*, 35: 27730–27744, 2022.
- Athanasios Papoulis. *Random variables and stochastic processes*. McGraw Hill, 1965.
- Mark Schmidt, Glenn Fung, and Romer Rosales. Optimization methods for l1-regularization. *University of British Columbia, Technical Report TR-2009-19*, 2009.
- Jeremy F Shapiro. A survey of lagrangean techniques for discrete optimization. In *Annals of Discrete Mathematics*, volume 5, pp. 113–138. Elsevier, 1979.

- 
- Nitish Srivastava, Geoffrey Hinton, Alex Krizhevsky, Ilya Sutskever, and Ruslan Salakhutdinov. Dropout: a simple way to prevent neural networks from overfitting. *The journal of machine learning research*, 15(1):1929–1958, 2014.
- Chunqi Wang, Bingchao Wu, Zheng Chen, Lei Shen, Bing Wang, and Xiaoyi Zeng. Scaling transformers for discriminative recommendation via generative pretraining. In *Proceedings of the 31st ACM SIGKDD Conference on Knowledge Discovery and Data Mining V. 2*, pp. 2893–2903, 2025.
- Minhui Xie, Kai Ren, Youyou Lu, Guangxu Yang, Qingxing Xu, Bihai Wu, Jiazhen Lin, Hongbo Ao, Wanhong Xu, and Jiwu Shu. Kraken: memory-efficient continual learning for large-scale real-time recommendations. In *SC20: International Conference for High Performance Computing, Networking, Storage and Analysis*, pp. 1–17. IEEE, 2020.
- Chiyuan Zhang, Samy Bengio, Moritz Hardt, Benjamin Recht, and Oriol Vinyals. Understanding deep learning requires rethinking generalization. *arXiv preprint arXiv:1611.03530*, 2016.
- Yuanxing Zhang, Langshi Chen, Siran Yang, Man Yuan, Huimin Yi, Jie Zhang, Jiamang Wang, Jianbo Dong, Yunlong Xu, Yue Song, et al. Picasso: Unleashing the potential of gpu-centric training for wide-and-deep recommender systems. In *2022 IEEE 38th International Conference on Data Engineering (ICDE)*, pp. 3453–3466. IEEE, 2022a.
- Zhao-Yu Zhang, Xiang-Rong Sheng, Yujing Zhang, Biye Jiang, Shuguang Han, Hongbo Deng, and Bo Zheng. Towards understanding the overfitting phenomenon of deep click-through rate models. In *Proceedings of the 31st ACM international conference on information & knowledge management*, pp. 2671–2680, 2022b.
- Guorui Zhou, Xiaoqiang Zhu, Chenru Song, Ying Fan, Han Zhu, Xiao Ma, Yanghui Yan, Junqi Jin, Han Li, and Kun Gai. Deep interest network for click-through rate prediction. In *Proceedings of the 24th ACM SIGKDD international conference on knowledge discovery & data mining*, pp. 1059–1068, 2018.
- Jieming Zhu, Quanyu Dai, Liangcai Su, Rong Ma, Jinyang Liu, Guohao Cai, Xi Xiao, and Rui Zhang. Bars: Towards open benchmarking for recommender systems. In *Proceedings of the 45th International ACM SIGIR Conference on Research and Development in Information Retrieval*, pp. 2912–2923, 2022.

---

## APPENDIX

### A GENAI USAGE DISCLOSURE

During the preparation of this work, the author used ChatGPT to improve the language. After using this tool, the author reviewed and edited the content as necessary and takes full responsibility for the final publication.

### B ADAGRAD WITH ADAPTIVE REGULARIZATION

Adagrad, like Adam, is widely used in the ASR domain. Our method extends readily to Adagrad, as detailed in Algorithm 2.

---

**Algorithm 2** Adagrad with Adaptive Regularization (AdagradAR)

---

- 1: given  $\varepsilon = 10^{-8}$ ,  $\alpha$ , learning rate  $\eta$
  - 2: initialize time step  $t \leftarrow 0$ , parameter  $\theta_p^{t=0}$ , squared gradient accumulator  $v_p^{t=0} \leftarrow 0$ , last update step state  $s_p^{t=0} \leftarrow 0$
  - 3: **repeat**
  - 4:    $t \leftarrow t + 1$
  - 5:    $g_p^t \leftarrow \nabla_{\theta_p} f(\theta_p^{t-1})$
  - 6:    $v_p^t \leftarrow v_p^{t-1} + (g_p^t)^2$
  - 7:    $\lambda_p^t \leftarrow \min(1, (t - s_p^{t-1} - 1) \alpha)$
  - 8:    $s_p^t \leftarrow t$  if  $\|g_p^t\| > 0$  else  $s_p^{t-1}$
  - 9:    $\theta_p^t \leftarrow \theta_p^{t-1} - \lambda_p^t \theta_p^{t-1} - \eta \cdot g_p^t / (\sqrt{v_p^t} + \varepsilon)$
  - 10: **until** stopping criterion is met
  - 11: return optimized parameters  $\theta_p^t$
- 

### C NETWORK ARCHITECTURE CONFIGURATIONS

We adjust the network architectures based on the feature and sample sizes of each dataset. As summarized in table 3, larger and deeper networks are utilized for datasets with more features and samples, such as iPinYou, Avazu, and LZD. In contrast, smaller and shallower networks are adopted for the Amazon dataset to mitigate the risk of overfitting.

Table 3: Network architecture configurations for different datasets

Dataset	DNN	WDL	DeepFM		WuKong			
	MLP Hidden Sizes	MLP Hidden Sizes	MLP Hidden Sizes	Layers	LCB Emb	FMB Emb	FMB Hiddens	MLP Hidden Sizes
iPinYou	[512, 256, 128]	[512, 256, 128]	[512, 256, 128]	5	12	12	[64, 32]	[512, 256, 128]
Amazon	[512, 256, 128]	[512, 256]	[512, 256]	1	8	8	[32, 32]	[512, 256]
Avazu	[512, 256, 128]	[512, 256, 128]	[512, 256, 128]	5	12	12	[64, 32]	[512, 256, 128]
LZD	[512, 256, 128]	[512, 256, 128]	[512, 256, 128]	5	12	12	[64, 32]	[512, 256, 128]

### D GRID SEARCH FOR THE WEIGHT DECAY COEFFICIENT

The weight decay coefficient is a crucial hyperparameter that significantly affects model performance. In our adaptive regularization method, the weight decay coefficient is denoted as  $\alpha$  in equation 11. To ensure a fair comparison across methods, we perform a grid search to select the optimal weight decay value for each dataset and model combination. Figure 3 illustrates the impact of varying the weight decay coefficient on test AUC for the Avazu dataset using a DNN backbone at the end of epoch 2. Although test AUC fluctuates with different values of the weight decay coefficient, our proposed method consistently achieves superior performance compared to AdamW and AdagradW. Furthermore, the performance of AdamW and AdagradW varies dramatically with the weight decay

coefficient, while our method demonstrates greater stability. This indicates that our method is less sensitive to the choice of weight decay coefficient, thereby simplifying hyperparameter tuning in practice.

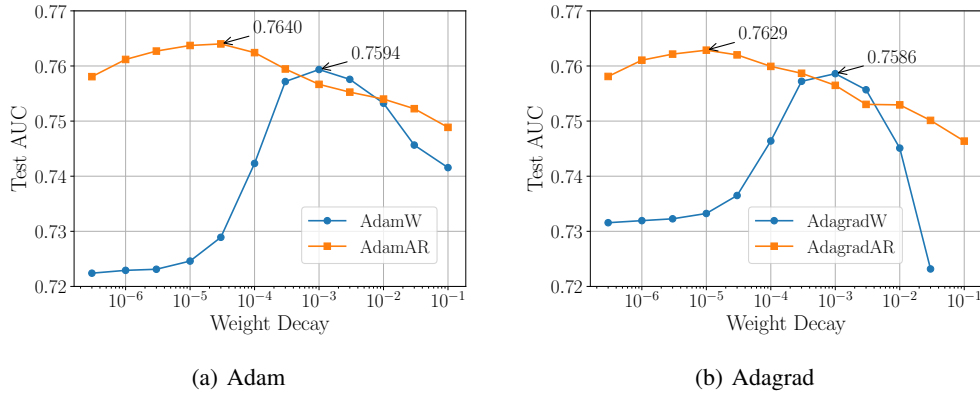


Figure 3: Performance of different weight decay coefficient on Avazu dataset with DNN backbone at the end of epoch 2. (a) shows the performance with Adam. (b) shows the performance with Adagrad.

## E FEATURE STATISTICS ON IPINYOU DATASET

The iPinYou dataset contains a total of 16 features, among which only a few are sparse. Table 4 lists the top six sparse features along with their statistical indicators.

Table 4: For the top six sparse features in the iPinYou dataset, the table below presents the number of unique IDs, the average occurrences of each ID, and the mean update interval for each ID with a batch size of 2048.

Feature	IP	slotid	domain	city	creative	useragent
Unique IDs	704,966	180,696	51,322	372	133	42
Mean Occurrences	27.7	107.9	379.9	52,408.5	146,586.3	464,189.9
Mean Update Intervals	344.222	88.230	25.060	0.182	0.065	0.021